

Solving Blind Inverse Problems: Adaptive Diffusion Models for Motion-Corrected Sparse-View 4DCT

Antoine De Paepe¹ Alexandre Bousse¹ Clémentine Phung-Ngoc¹ Dimitris Visvikis¹

¹University of Western Brittany, LaTIM, UMR Inserm 1101, 29238 Brest, France

Fully 3D 2025, Shanghai, China - May 27, 2025



Introduction

Introduction to Lung CT

- **Lung CT Reconstruction:** The reconstruction of lung CT images can be formulated as the following optimization problem:

$$\min_{\mathbf{x}} \frac{1}{2} \|\mathcal{R}\mathbf{x} - \mathbf{b}\|_W^2 + \mathcal{R}(\mathbf{x})$$

Introduction to Lung CT

- **Lung CT Reconstruction:** The reconstruction of lung CT images can be formulated as the following optimization problem:

$$\min_{\mathbf{x}} \frac{1}{2} \|\mathcal{R}\mathbf{x} - \mathbf{b}\|_W^2 + \mathcal{R}(\mathbf{x})$$

- **Limitations of Static CT:**

- Assumes the patient remains stationary during the scan.
- Respiratory motion can introduce artifacts and blurring.

Introduction to Lung CT

- **Lung CT Reconstruction:** The reconstruction of lung CT images can be formulated as the following optimization problem:

$$\min_{\mathbf{x}} \frac{1}{2} \|\mathcal{R}\mathbf{x} - \mathbf{b}\|_W^2 + \mathbf{R}(\mathbf{x})$$

- **Limitations of Static CT:**

- Assumes the patient remains stationary during the scan.
- Respiratory motion can introduce artifacts and blurring.

- **Introduction to 4DCT:**

- Captures 3D images across respiratory phases, enabling dynamic lung motion visualization.
- Essential for applications like radiotherapy planning [Kwong et al. 2015].

Introduction to Dynamic Lung CT

- **4DCT Acquisition Modes:**

- Helical mode: The scanner rotates continuously as the patient table moves through the gantry.
- Cine mode: The scanner acquires multiple images at the same table position over a period.
- Uses a surrogate signal (e.g., respiratory belt or external marker) to track breathing motion.

Introduction to Dynamic Lung CT

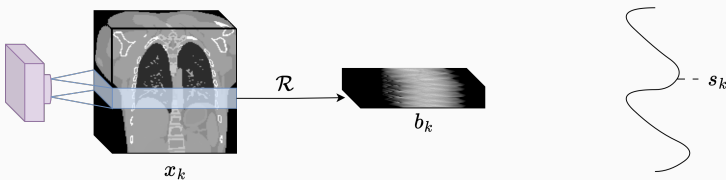
- **4DCT Acquisition Modes:**
 - Helical mode: The scanner rotates continuously as the patient table moves through the gantry.
 - Cine mode: The scanner acquires multiple images at the same table position over a period.
 - Uses a surrogate signal (e.g., respiratory belt or external marker) to track breathing motion.
- **Example of Helical 4DCT Acquisition:**

Introduction to Dynamic Lung CT

- **4DCT Acquisition Modes:**

- Helical mode: The scanner rotates continuously as the patient table moves through the gantry.
- Cine mode: The scanner acquires multiple images at the same table position over a period.
- Uses a surrogate signal (e.g., respiratory belt or external marker) to track breathing motion.

- **Example of Helical 4DCT Acquisition:**

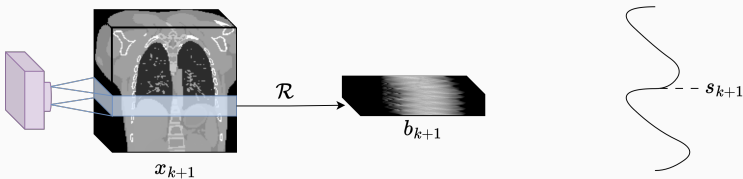


Introduction to Dynamic Lung CT

- **4DCT Acquisition Modes:**

- Helical mode: The scanner rotates continuously as the patient table moves through the gantry.
- Cine mode: The scanner acquires multiple images at the same table position over a period.
- Uses a surrogate signal (e.g., respiratory belt or external marker) to track breathing motion.

- **Example of Helical 4DCT Acquisition:**

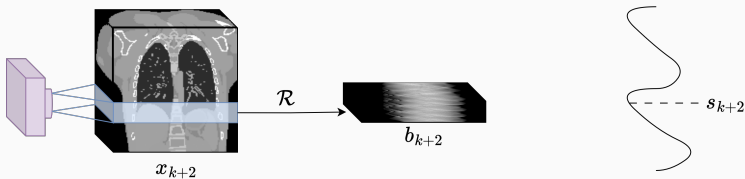


Introduction to Dynamic Lung CT

- **4DCT Acquisition Modes:**

- Helical mode: The scanner rotates continuously as the patient table moves through the gantry.
- Cine mode: The scanner acquires multiple images at the same table position over a period.
- Uses a surrogate signal (e.g., respiratory belt or external marker) to track breathing motion.

- **Example of Helical 4DCT Acquisition:**

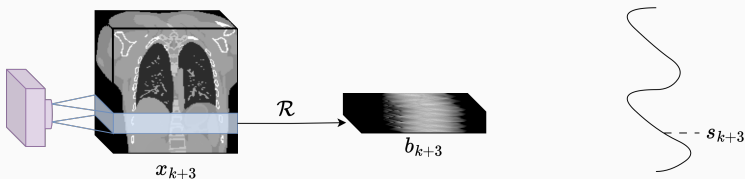


Introduction to Dynamic Lung CT

- **4DCT Acquisition Modes:**

- Helical mode: The scanner rotates continuously as the patient table moves through the gantry.
- Cine mode: The scanner acquires multiple images at the same table position over a period.
- Uses a surrogate signal (e.g., respiratory belt or external marker) to track breathing motion.

- **Example of Helical 4DCT Acquisition:**



Challenges in 4DCT

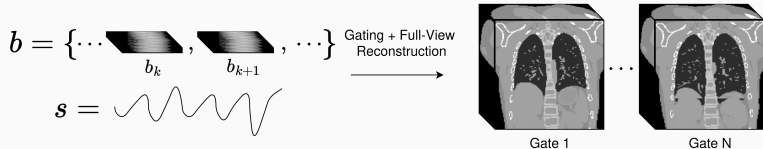
$$b = \{\dots, \overbrace{b_k}, \overbrace{b_{k+1}}, \dots\}$$

$$s = \text{wavy line}$$

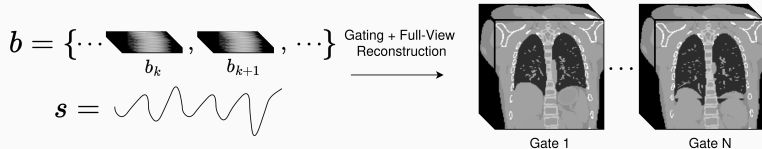
Challenges in 4DCT

$$b = \{\dots, b_k, b_{k+1}, \dots\} \xrightarrow{\text{Gating + Full-View Reconstruction}} s = \text{wavy line}$$

Challenges in 4DCT



Challenges in 4DCT



- **Challenges:**

- Motion artifacts due to irregular breathing patterns.
- Surrogate signals may not always be stored.
- Increased radiation dose from multiple phase acquisitions;
necessitates dose reduction strategies.

Joint Reconstruction & Motion Estimation (JRM)

- General JRM Framework:

$$\min_{\boldsymbol{x}, \varphi} \frac{1}{2} \|\mathcal{A}_{\varphi} \boldsymbol{x} - \boldsymbol{b}\|_W^2 + \boldsymbol{R}(\boldsymbol{x})$$

where φ are motion parameters.

Joint Reconstruction & Motion Estimation (JRM)

- General JRM Framework:

$$\min_{\mathbf{x}, \varphi} \frac{1}{2} \|\mathcal{A}_\varphi \mathbf{x} - \mathbf{b}\|_W^2 + \mathbf{R}(\mathbf{x})$$

where φ are motion parameters.

- 4DCT JRM Framework [Huang et al. 2024]:

$$\min_{\mathbf{x}, \varphi, \mathbf{s}} \frac{1}{2} \sum_{k=1}^{n_t} \|\mathcal{R} \circ \mathcal{T}_k \circ \mathcal{W}_{\varphi \cdot \mathbf{s}_k} \mathbf{x} - \mathbf{b}_k\|_W^2 + \mathbf{R}(\mathbf{x})$$

where φ, \mathbf{s} are deformation vector fields parametrized by B-spline grid and surrogate signals.

Joint Reconstruction & Motion Estimation (JRM)

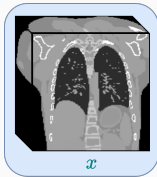
- General JRM Framework:

$$\min_{\boldsymbol{x}, \boldsymbol{\varphi}} \frac{1}{2} \|\mathcal{A}_{\boldsymbol{\varphi}} \boldsymbol{x} - \boldsymbol{b}\|_W^2 + \mathbf{R}(\boldsymbol{x})$$

where $\boldsymbol{\varphi}$ are motion parameters.

- 4DCT JRM Framework [Huang et al. 2024]:

$$\min_{\boldsymbol{x}, \boldsymbol{\phi}, \boldsymbol{s}} \frac{1}{2} \sum_{k=1}^{n_t} \|\mathcal{R} \circ \mathcal{T}_k \circ \mathcal{W}_{\boldsymbol{\phi} \cdot \boldsymbol{s}_k} \boldsymbol{x} - \boldsymbol{b}_k\|_W^2 + \mathbf{R}(\boldsymbol{x})$$



where $\boldsymbol{\phi}, \boldsymbol{s}$ are deformation vector fields parametrized by B-spline grid and surrogate signals.

Joint Reconstruction & Motion Estimation (JRM)

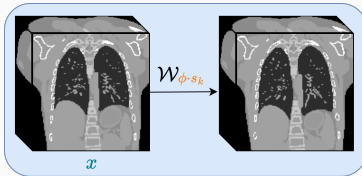
- General JRM Framework:

$$\min_{\boldsymbol{x}, \boldsymbol{\varphi}} \frac{1}{2} \|\mathcal{A}_{\boldsymbol{\varphi}} \boldsymbol{x} - \boldsymbol{b}\|_W^2 + \mathcal{R}(\boldsymbol{x})$$

where $\boldsymbol{\varphi}$ are motion parameters.

- 4DCT JRM Framework [Huang et al. 2024]:

$$\min_{\boldsymbol{x}, \boldsymbol{\phi}, \boldsymbol{s}} \frac{1}{2} \sum_{k=1}^{n_t} \|\mathcal{R} \circ \mathcal{T}_k \circ \mathcal{W}_{\boldsymbol{\phi} \cdot \boldsymbol{s}_k} \boldsymbol{x} - \boldsymbol{b}_k\|_W^2 + \mathcal{R}(\boldsymbol{x})$$



where $\boldsymbol{\phi}, \boldsymbol{s}$ are deformation vector fields parametrized by B-spline grid and surrogate signals.

Joint Reconstruction & Motion Estimation (JRM)

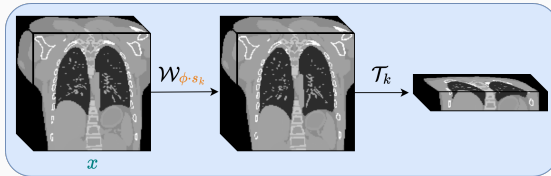
- General JRM Framework:

$$\min_{\mathbf{x}, \boldsymbol{\varphi}} \frac{1}{2} \|\mathcal{A}_{\boldsymbol{\varphi}} \mathbf{x} - \mathbf{b}\|_W^2 + \mathbf{R}(\mathbf{x})$$

where $\boldsymbol{\varphi}$ are motion parameters.

- 4DCT JRM Framework [Huang et al. 2024]:

$$\min_{\mathbf{x}, \boldsymbol{\phi}, \mathbf{s}} \frac{1}{2} \sum_{k=1}^{n_t} \|\mathcal{R} \circ \mathcal{T}_k \circ \mathcal{W}_{\boldsymbol{\phi} \cdot \mathbf{s}_k} \mathbf{x} - \mathbf{b}_k\|_W^2 + \mathbf{R}(\mathbf{x})$$



where $\boldsymbol{\phi}, \mathbf{s}$ are deformation vector fields parametrized by B-spline grid and surrogate signals.

Joint Reconstruction & Motion Estimation (JRM)

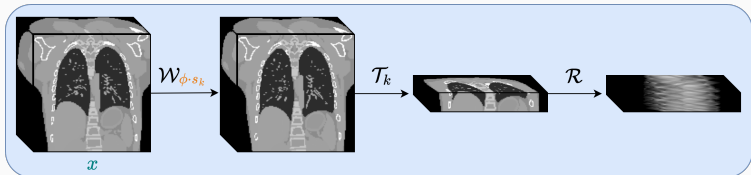
- General JRM Framework:

$$\min_{\mathbf{x}, \boldsymbol{\varphi}} \frac{1}{2} \|\mathcal{A}_{\boldsymbol{\varphi}} \mathbf{x} - \mathbf{b}\|_W^2 + \mathcal{R}(\mathbf{x})$$

where $\boldsymbol{\varphi}$ are motion parameters.

- 4DCT JRM Framework [Huang et al. 2024]:

$$\min_{\mathbf{x}, \boldsymbol{\phi}, \mathbf{s}} \frac{1}{2} \sum_{k=1}^{n_t} \|\mathcal{R} \circ \mathcal{T}_k \circ \mathcal{W}_{\boldsymbol{\phi} \cdot \mathbf{s}_k} \mathbf{x} - \mathbf{b}_k\|_W^2 + \mathcal{R}(\mathbf{x})$$



where $\boldsymbol{\phi}, \mathbf{s}$ are deformation vector fields parametrized by B-spline grid and surrogate signals.

Methods

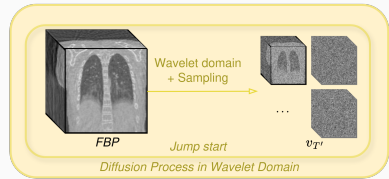
Challenges and Proposed Solution

- **Challenges:**
 - Sparse-view data increases the ill-posedness of the problem.
 - Hand-crafted regularizers (e.g., Total Variation) tend to oversmooth and erase subtle image features.

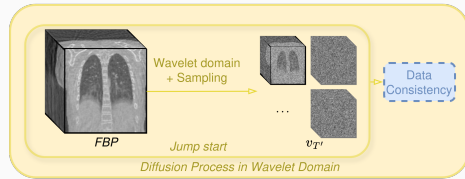
Challenges and Proposed Solution

- **Challenges:**
 - Sparse-view data increases the ill-posedness of the problem.
 - Hand-crafted regularizers (e.g., Total Variation) tend to oversmooth and erase subtle image features.
- **Solution Overview:**
 - JRM via Adaptive Diffusion Models (ADMs).
 - Motion-free \mathbf{x} is estimated via a Deep Posterior Sampling (DPS) approach [Zhu et al. 2023].
 - Motion parameters ϕ, \mathbf{s} are estimated through a classical optimization pipeline.
 - Wavelet Diffusion Models (WDMs) [Friedrich et al. 2024] are used to enhance computational efficiency.

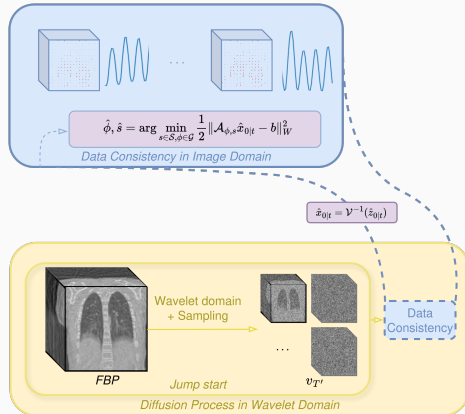
Overview of JRM-ADM



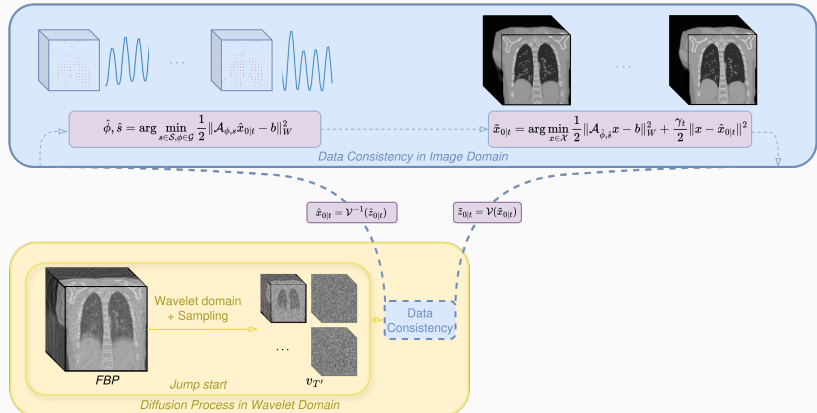
Overview of JRM-ADM



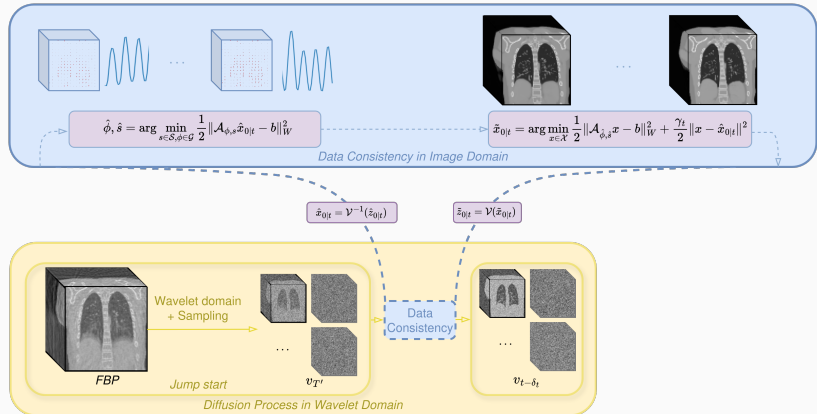
Overview of JRM-ADM



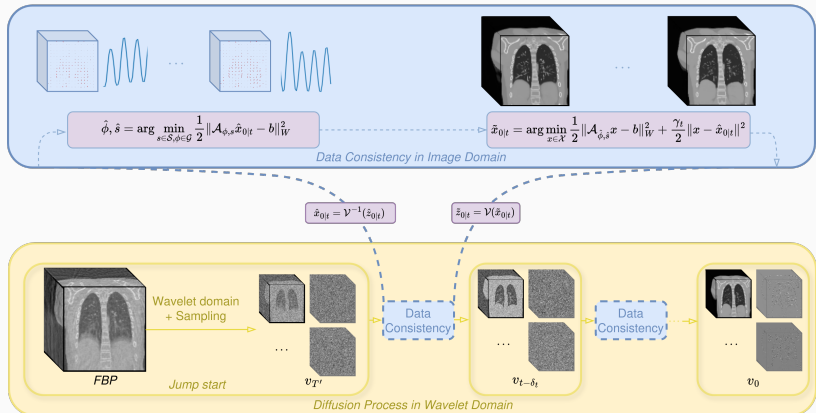
Overview of JRM-ADM



Overview of JRM-ADM



Overview of JRM-ADM



Experiments

Quantitative Results

Experiments on XCAT

Phantoms:

- Generated 3D thorax CT volumes (128^3 voxels, 2.6^3 mm^3 voxel size) using the XCAT phantoms [Segars et al. 2010].
- Trained WDMs on these volumes to learn anatomical priors.
- Simulated sparse-view 4DCT acquisitions with 52 projection angles.

Quantitative Results

Experiments on XCAT Phantoms:

- Generated 3D thorax CT volumes (128^3 voxels, 2.6^3 mm^3 voxel size) using the XCAT phantoms [Segars et al. 2010].
- Trained WDMs on these volumes to learn anatomical priors.
- Simulated sparse-view 4DCT acquisitions with 52 projection angles.

Experiments on Pseudo-Real Data:

- Using LIDC-IDRI [Armato III et al. 2011] 3D thorax CT volumes (256^3 voxels, 1.25^3 mm^3 voxel size)
- Trained WDMs on these volumes to learn anatomical priors.
- Simulated sparse-view 4DCT acquisitions on CHRU CT volumes with 52 projection angles using a CT respiratory motion synthesis framework [Cao et al. 2024].

Quantitative Results

Experiments on XCAT Phantoms:

- Generated 3D thorax CT volumes (128^3 voxels, 2.6^3 mm^3 voxel size) using the XCAT phantoms [Segars et al. 2010].
- Trained WDMs on these volumes to learn anatomical priors.
- Simulated sparse-view 4DCT acquisitions with 52 projection angles.
- **Evaluation:** Assessed reconstruction quality using metrics such as SSIM and PSNR.

Experiments on Pseudo-Real Data:

- Using LIDC-IDRI [Armato III et al. 2011] 3D thorax CT volumes (256^3 voxels, 1.25^3 mm^3 voxel size)
- Trained WDMs on these volumes to learn anatomical priors.
- Simulated sparse-view 4DCT acquisitions on CHRU CT volumes with 52 projection angles using a CT respiratory motion synthesis framework [Cao et al. 2024].

Quantitative Evaluation of Reconstruction Methods

| Metric | Gated FBP | Gated DPS | JRM-TV | JRM-ADM |
|--------|-----------|-----------|--------|--------------|
| PSNR ↑ | 20.59 | 24.09 | 25.04 | 27.05 |
| SSIM ↑ | 0.37 | 0.90 | 0.89 | 0.94 |

Table 1: Quantitative evaluation (PSNR, SSIM) of four different reconstruction methods on the end-inhale phase for five XCAT phantoms.

Qualitative Evaluation of Reconstruction Methods

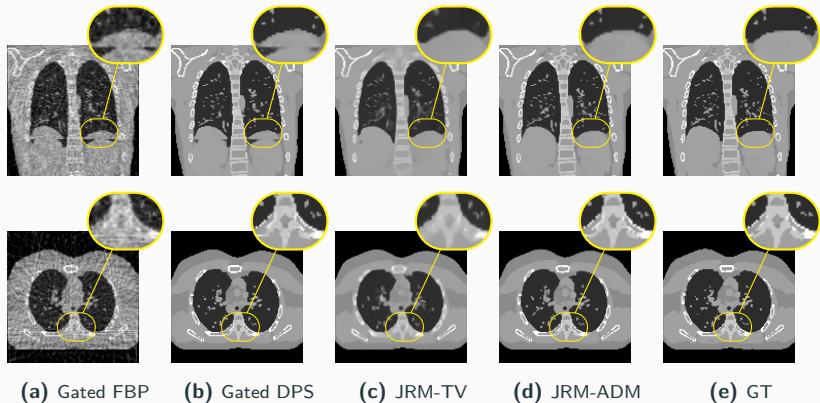


Figure 1: GT and end-inhale phase reconstructions on XCAT phantoms.

Qualitative Evaluation of Reconstruction Methods

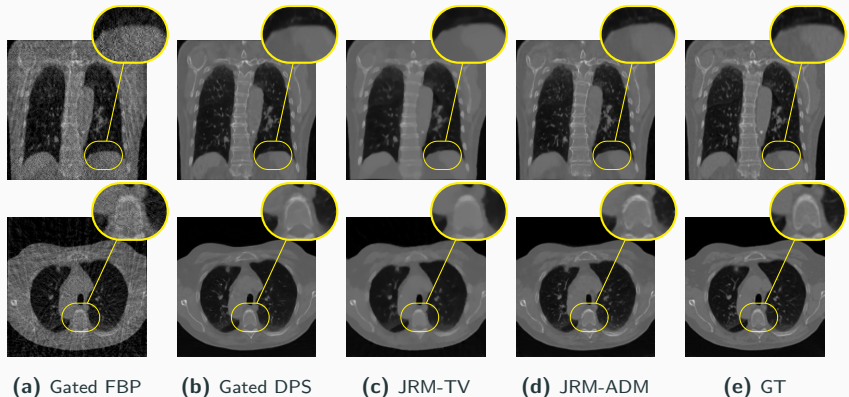


Figure 2: GT and reconstructions on pseudo-real data.

Qualitative Evaluation of Reconstruction Methods

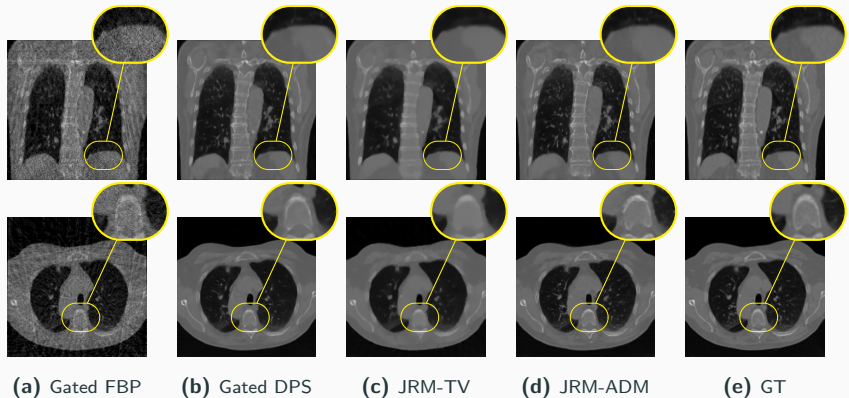


Figure 2: GT and reconstructions on pseudo-real data.

Qualitative Evaluation of Reconstruction Methods

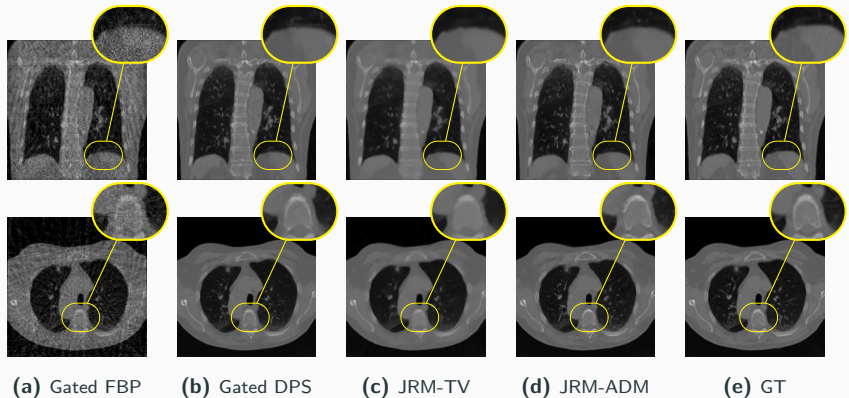


Figure 2: GT and reconstructions on pseudo-real data.

Qualitative Evaluation of Reconstruction Methods

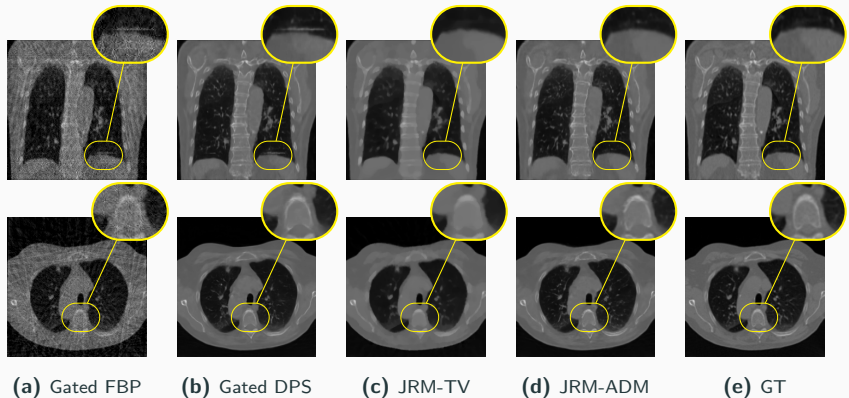


Figure 2: GT and reconstructions on pseudo-real data.

Qualitative Evaluation of Reconstruction Methods

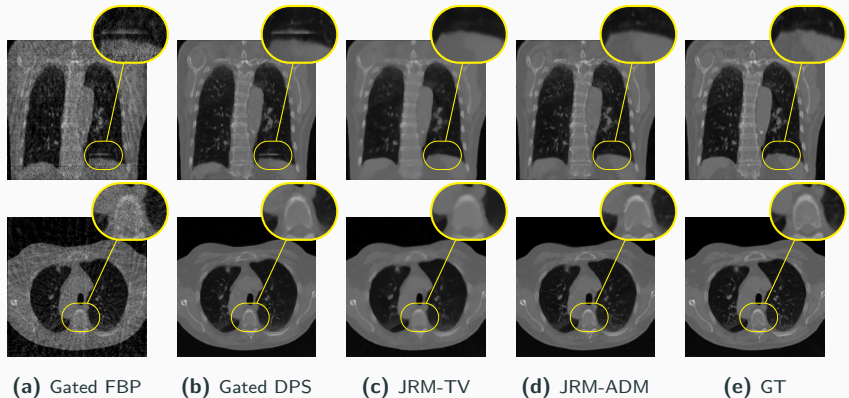


Figure 2: GT and reconstructions on pseudo-real data.

Qualitative Evaluation of Reconstruction Methods

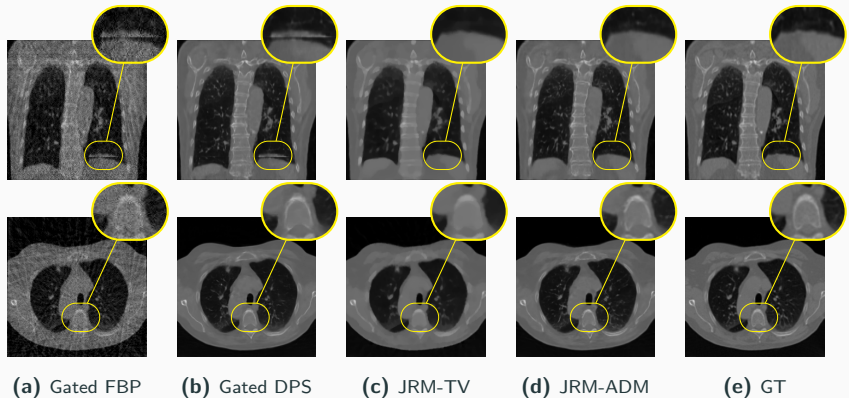


Figure 2: GT and reconstructions on pseudo-real data.

Qualitative Evaluation of Reconstruction Methods

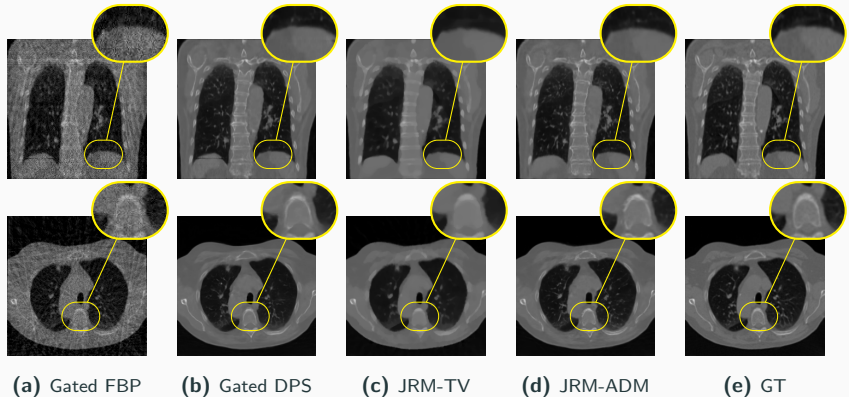


Figure 2: GT and reconstructions on pseudo-real data.

Qualitative Evaluation of Reconstruction Methods

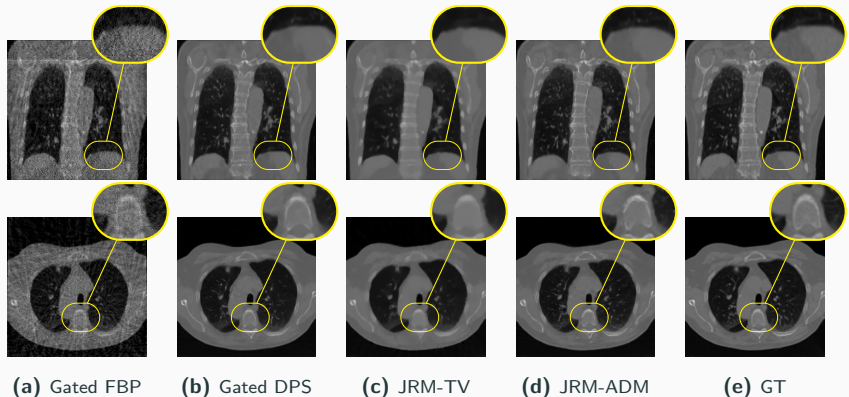


Figure 2: GT and reconstructions on pseudo-real data.

Qualitative Evaluation of Reconstruction Methods

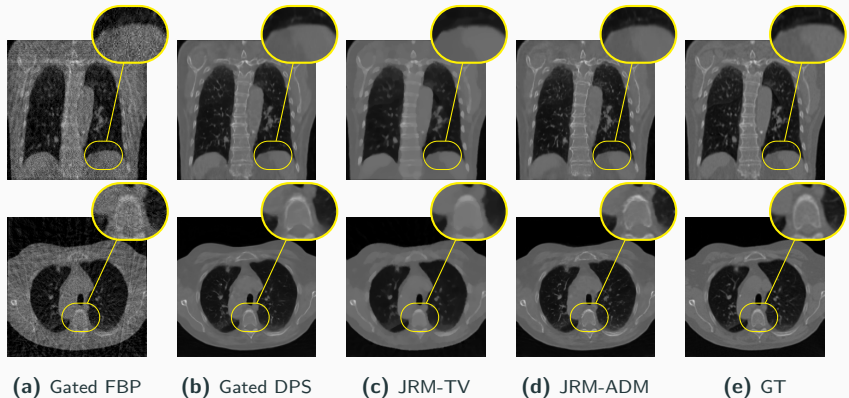


Figure 2: GT and reconstructions on pseudo-real data.

Qualitative Evaluation of Reconstruction Methods

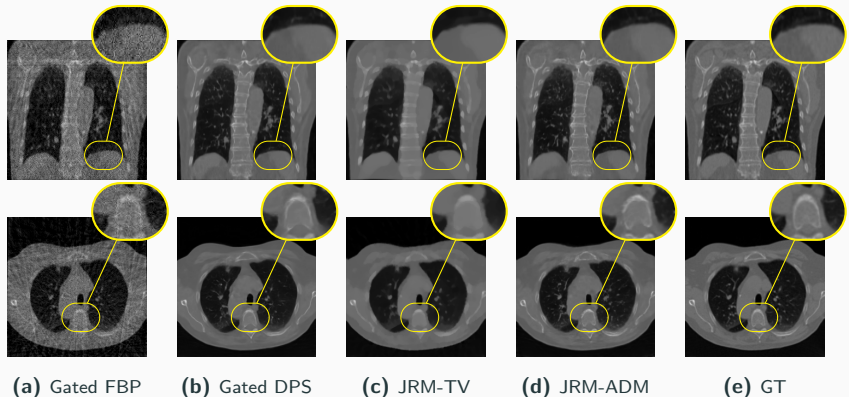


Figure 2: GT and reconstructions on pseudo-real data.

Extension to Motion-Corrected Sparse-View Head CBCT

[De Paepe et al. 2025]: Quantitative Results

| Views | Method | PSNR (\uparrow) | SSIM (\uparrow) | MAE τ (\downarrow) | MAE ϑ (\downarrow) |
|-------|---------|---------------------|---------------------|-----------------------------|----------------------------------|
| 60 | FDK | 17.00 | 0.23 | - | - |
| | JRM-TV | 28.91 | 0.90 | 0.34 | 0.11 |
| | JRM-ADM | 29.67 | 0.92 | 0.27 | 0.09 |
| 40 | FDK | 16.92 | 0.19 | - | - |
| | JRM-TV | 27.19 | 0.87 | 0.43 | 0.12 |
| | JRM-ADM | 28.66 | 0.91 | 0.29 | 0.11 |
| 20 | FDK | 14.96 | 0.14 | - | - |
| | JRM-TV | 23.38 | 0.75 | 0.86 | 0.17 |
| | JRM-ADM | 27.18 | 0.87 | 0.30 | 0.12 |

Table 2: Quantitative results of methods in comparison on the CQ500 [Chilamkurthy et al. 2018] dataset for the motion corrected reconstruction tasks under sparse-view settings of 60, 40, and 20 views.

Extension to Motion-Corrected Sparse-View Head CBCT

[De Paepe et al. 2025]: Qualitative Results

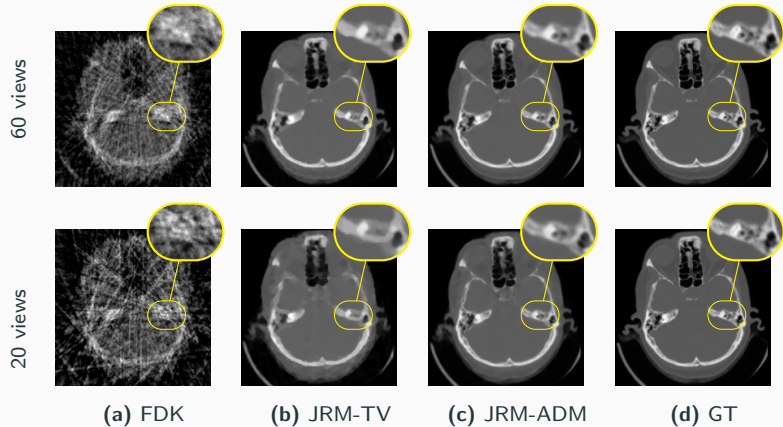


Figure 3: GT and reconstructions (axial plane) for motion-affected sparse-view CBCT: results are shown for 40- and 20-view acquisition settings.

Conclusion - Discussion

Conclusion & Discussion

- **High-fidelity 4DCT:** JRM-ADM yields artifact-free, high-resolution reconstructions under irregular breathing, outperforming classical reconstruction methods.

Conclusion & Discussion

- **High-fidelity 4DCT:** JRM-ADM yields artifact-free, high-resolution reconstructions under irregular breathing, outperforming classical reconstruction methods.
- **Computational Challenges:** GPU memory and runtime remain high; future work should explore how to solve this.

Conclusion & Discussion

- **High-fidelity 4DCT:** JRM-ADM yields artifact-free, high-resolution reconstructions under irregular breathing, outperforming classical reconstruction methods.
- **Computational Challenges:** GPU memory and runtime remain high; future work should explore how to solve this.
- **Real World Challenges:** Working on real sinograms would be the best path toward clinical translation.

Acknowledgments

This work was supported by the French **National Institute of Health and Medical Research (Inserm)**, by the **University of Western Brittany (UBO)**, by **France Life Imaging** under grant No ANR-11-INBS-0006 and by **CPER 2021–2027 IMAGIIS (INNOV-XS)**.



Université de Bretagne Occidentale



References i

-  Armato III, Samuel G et al. [2011]. “The lung image database consortium (LIDC) and image database resource initiative (IDRI): a completed reference database of lung nodules on CT scans”. In: *Medical physics* 38.2, pp. 915–931.
-  Cao, Yi-Heng et al. [2024]. “CT respiratory motion synthesis using joint supervised and adversarial learning”. In: *Physics in Medicine & Biology* 69.9, p. 095001.
-  Chilamkurthy, Sasank et al. [2018]. “Deep learning algorithms for detection of critical findings in head CT scans: a retrospective study”. In: *The Lancet* 392.10162, pp. 2388–2396.
-  De Paepe, Antoine et al. [2025]. “Adaptive Diffusion Models for Sparse-View Motion-Corrected Head Cone-beam CT”. In: *arXiv e-prints*, arXiv–2504.
-  Friedrich, Paul et al. [2024]. “Wdm: 3d wavelet diffusion models for high-resolution medical image synthesis”. In: *MICCAI Workshop on Deep Generative Models*. Springer, pp. 11–21.
-  Huang, Yuliang et al. [2024]. “Resolving Variable Respiratory Motion From Unsorted 4D Computed Tomography”. In: *International Conference on Medical Image Computing and Computer-Assisted Intervention*. Springer, pp. 588–597.

References ii

-  Kwong, Yune et al. [2015]. “Four-dimensional computed tomography (4DCT): a review of the current status and applications”. In: *Journal of medical imaging and radiation oncology* 59.5, pp. 545–554.
-  Segars, W Paul et al. [2010]. “4D XCAT phantom for multimodality imaging research”. In: *Medical physics* 37.9, pp. 4902–4915.
-  Zhu, Yuanzhi et al. [2023]. “Denoising diffusion models for plug-and-play image restoration”. In: *Proceedings of the IEEE/CVF Conference on Computer Vision and Pattern Recognition*, pp. 1219–1229.